

# COHERENT VORTEX EXTRACTION IN ROTATING AND STRATIFIED TURBULENCE

L. Liechtenstein<sup>1,\*</sup>, F.S. Godeferd<sup>2</sup>, C. Cambon<sup>2</sup>, M. Farge<sup>3</sup> and K. Schneider<sup>1</sup>

<sup>1</sup>MSNM-CNRS & CMI, Université de Provence, Marseille, France

<sup>2</sup>Laboratoire de Mécanique des Fluides et d'Acoustique, Ecole Centrale de Lyon, France

<sup>3</sup>Laboratoire de Météorologie Dynamique du CNRS, Ecole Normale Supérieure, Paris, France

\*Email: lukas.liechtenstein@ec-lyon.fr

## Abstract

*We apply a wavelet based coherent vortex extraction (CVE) method to DNS data of stratified and rotating homogeneous turbulence. We find that 1% of the strongest wavelet coefficients represent the coherent vortices of the flow, retaining almost all of the enstrophy and energy ( 99.9 % ). The statistics of the coherent flow is quasi-identical to the one of the total flow. Compared to isotropic turbulence, the anisotropic case shows a reduced incoherent part.*

## INTRODUCTION

A good understanding of rotating and stratified turbulence is important for modelling geophysical flows, like prediction of energy, dissipation or mixing and transport of scalars. In this paper we analyse incompressible turbulence taking into account both rotation and stratification in a ratio of  $\alpha = f/N = 0.2$ , where  $f$  is the Coriolis parameter and  $N$  the Brunt-Vaissälä frequency. The incompressible Navier-Stokes equations are solved using the Boussinesq approximation [1]. The Coriolis force as well as the buoyancy force act linearly on the velocity field, creating inertio-gravity waves. The existence of these internal waves due to rotation and stratification give rise to linear mechanisms which are well known (see e.g. [1,2]). However, the nonlinear evolution leading to the formation of coherent vortices is significantly more complicated [1,3,4], including interactions between a non-propagating vortex mode and waves. In this paper we analyse anisotropic turbulence at one time instant, calculated with direct numerical simulation (DNS). The aim is to identify the effect of partial linearisation through rotation and stratification by comparing the field

with a similar one of isotropic turbulence.

The DNS data is calculated with a fully de-aliased, pseudo-spectral code using a Fourier basis with periodic boundary conditions and a resolution of  $n = 540^3$ . The time scheme is third-order Adams-Bashforth with exact integration of the viscous term. The simulation is initialised by an isotropic fully developed turbulent field. This isotropic pre-computation is itself initialised with a narrow-band spectrum with the energy peak at wave number  $k = 12$ . The subsequent simulation is also freely decaying. Two simulations have been carried out, run A corresponds to rotating and stratified turbulence while run B corresponds to isotropic. The latter is shown here for comparison. As both flows are freely decaying, the Reynolds numbers are significantly smaller than for forced ones computed at the same resolution. Different parameters of the runs are assembled in table 1. The time instant of the runs have been chosen so that the analysed fields contain approximately the same amount of turbulent kinetic energy. In terms of initial turbulent turnover times  $T_L = tu/L$ ,

	Run A	Run B
$2\Omega = f$	$\pi$	0
$N$	$5\pi$	0
Energy $E$	0.0139	0.0142
Enstrophy $Z$	1.07	5.403
Viscosity $\nu$	$3.33 \cdot 10^{-4}$	$3.33 \cdot 10^{-4}$
$R_\lambda$	125	56
$T_f = ft/2\pi$	5	-
$T_L = tu/L$	9.2	2.8

Table 1

Parameters and statistical properties of run A (anisotropic) and run B (isotropic) at times  $T_L = 9.2$  and  $T_L = 2.8$ , respectively.

where  $u$  and  $L$  are the initial mean velocity fluctuation and integral scale respectively, run A has been analysed at time  $T_L = 9.2$  while run B at  $T_L = 2.8$  (see table 1). Therefore, the time instant for the anisotropic flow is chosen later, as rotating and stratified turbulence decays slower than isotropic turbulence. Although the kinetic energies of the two runs are approximately equal, the Taylor micro-scales  $\lambda = \sqrt{5E/Z}$  of runs A and B differ. The isotropic run thereby shows a significantly smaller Reynolds number  $R_\lambda$  than the anisotropic one.

In [5] an orthogonal wavelet-based method to extract coherent vortices (CVE) out of 3D turbulent flows was proposed. The principle is to split the flow into two parts, a coherent and an incoherent one. For this, the vorticity field is transformed into wavelet space (see e.g.[7]) and a non-linear thresholding is applied to the wavelet coefficients. The coherent vorticity is reconstructed from the strongest coefficients while the incoherent one is reconstructed from the remaining weak coefficients. The threshold  $\epsilon_T = (\frac{4}{3}Z \log n)^{1/2}$  depends only on the total enstrophy  $Z$  and on the resolution  $n$  and is motivated by Donoho's theorem for signal de-noising.

For the orthogonal wavelet decomposition we use Coiflets of length 30 which have 10 vanishing moments [7]. This choice is motivated by the fact that the anisotropic flow exhibits a rapidly

decaying spectrum and hence a higher regularity of the wavelets is required, compared to previous applications of CVE, where Coiflets of length 12 have been used [5].

The decomposition yields for the vorticity  $\omega = \omega_c + \omega_i$ . Due to orthogonality, we have  $\langle \omega_c, \omega_i \rangle = 0$  and hence it follows that enstrophy is conserved,  $Z = Z_c + Z_i$ . The corresponding induced velocities,  $v = v_c + v_i$  are reconstructed using the Biot-Savart kernel. For the energy we get  $E = E_c + E_i + \epsilon$ , where epsilon remains small, 0.008 % for run B and 0.1% for run A, as shown in tables 2 and 3.

## RESULTS

Strat. & rot.	Total	Coherent	Incoh.
% of coeffs.	100%	1.0%	99.0%
Enstrophy	1.07052	1.06906	0.00146
% of enst.	100%	99.86%	0.14%
Vort. skewn.	0.0465	0.0465	-0.00091
Vort. flatn.	3.485	3.483	4.806
Energy	0.0138668	0.0138653	$2.37 \cdot 10^{-7}$
% of energy	100%	99.99%	0.002%
Vel. skewn.	0.0256	0.0250	0.00066
Vel. flatn.	3.613	3.614	3.474

Table 2

Statistical properties of the total, coherent and incoherent flows of run A at time  $T_L = 9.2$ .

Isotropic	Total	Coherent	Incoh.
% of coeffs.	100%	2.8%	97.2%
Enstrophy	5.40309	5.27969	0.12340
% of enst.	100%	97.72%	2.28%
Vort. skewn.	-0.00647	-0.00665	-0.00015
Vort. flatn.	5.041	5.025	3.985
Energy	0.014214	0.014190	$9.82 \cdot 10^{-6}$
% of energy	100%	99.83%	0.07%
Vel. skewn.	0.00394	-0.00441	-0.00057
Vel. flatn.	2.923	2.923	3.336

Table 3

Statistical properties of the total, coherent and incoherent flows of run B at time  $T_L = 2.8$ .

As seen in table 2, the coherent part obtained by applying CVE to run A, corresponding to 1% of the wavelet coefficients, retains nearly all of

the energy and enstrophy. The spectra, figures 1 and the vorticity PDF, figures 3 can barely be distinguished. Therefore the coherent flow is almost identical to the total one. Hence, only the coherent and the incoherent flows are shown in figures 2. The compression rate is defined as the fraction of retained wavelet coefficients for the coherent part and therefore measures its coherency. The CVE applied to anisotropic turbulence yields better results in terms of compression than those obtained for isotropic turbulence, despite the lower Reynolds number of the isotropic case. This confirms a higher degree of coherence in anisotropic turbulence, induced by the effect of stratification and rotation, which both appear as linear terms in the Navier-Stokes equations.

The spectral distributions shown in figures 1(a) and (b) show the different spectral decay rates of isotropic and anisotropic turbulence. The inhibited cascade and the steeper decay of the spectrum for anisotropic turbulence give rise to a larger Taylor micro scale than in isotropic turbulence with similar energy. This partially explains why the coherent structures in anisotropic turbulence differ qualitatively from those found in isotropic turbulence. Compared to isotropic turbulence, the coherency of anisotropic turbulence is larger, reflected by the higher compression rate seen in tables 2 and 3, despite the larger Reynolds number of the anisotropic case. The slower temporal decay of anisotropic turbulence associated with a steeper decay in the spectrum is a well known fact, revisited in [1,3,4] and attributed to a complex two-mode (wave-vortex) anisotropic cascading process. The spectra shown in figures 1 are a spherical average of the actual anisotropic 3D spectral distribution of turbulent energy.

The statistics of the incoherent parts in runs A and B differ to previous CVE's of isotropic turbulence at higher  $R_\lambda$  [5,6]. The incoherent parts in runs A and B show a slope of  $k^5$  instead of  $k^2$ . The reasons can be twofold, either due to the different

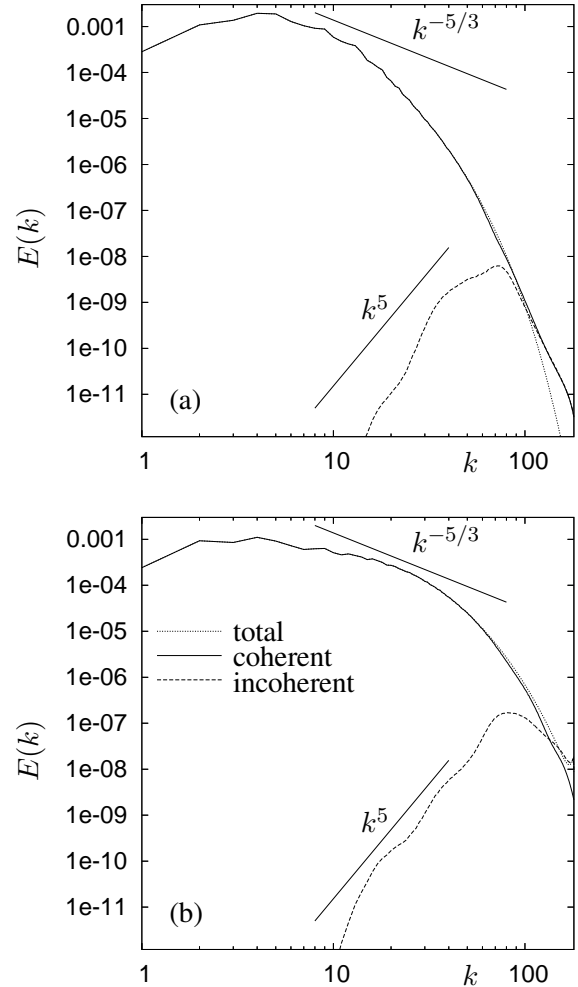


Figure 1. Energy spectra  $E(k)$  for the total, coherent and incoherent fields of (a) run A (anisotropic) and (b) run B (isotropic).

Reynolds number or due to the decaying nature of the here analysed flow. However, it seems that the behaviour of the incoherent part is independent of anisotropy present in the field.

The visualisations of the coherent and incoherent vorticity fields given in figures 2(a) and (b) show iso-surfaces of the magnitude of the vorticity. Note that the value of the iso-surface of the incoherent part is 15 times smaller than the one of the coherent part. We only show a sub-cube of the total calculation box (1/64th of the total box). In figure 2(a), one clearly identifies coherent structures which are qualitatively different from bent vortex tubes, often observed in isotropic turbu-

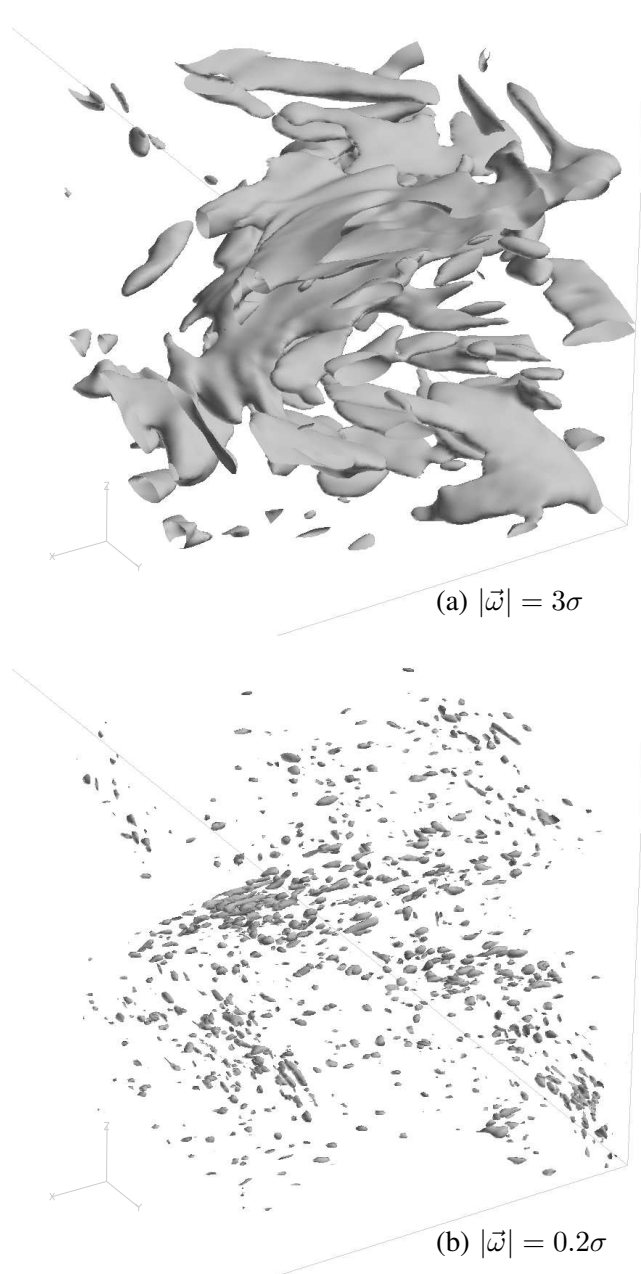


Figure 2. A sub-cube of  $128^3$  of the whole calculation domain. Coherent (a) and incoherent (b) vorticity ( $|\vec{\omega}| = 3\sigma$  for the coh. field and  $|\vec{\omega}| = 0.5\sigma$  for the incoh. field, with  $\sigma$  the stand. dev. of tot. vort.).

lence (see e.g. [5]). Note, that the structures are also different from pancake like structures observed in purely stratified turbulence [3]. The influence of rotation in the flow is therefore not negligible, even if stratification is dominant.

The vorticity PDFs of the coherent fields are

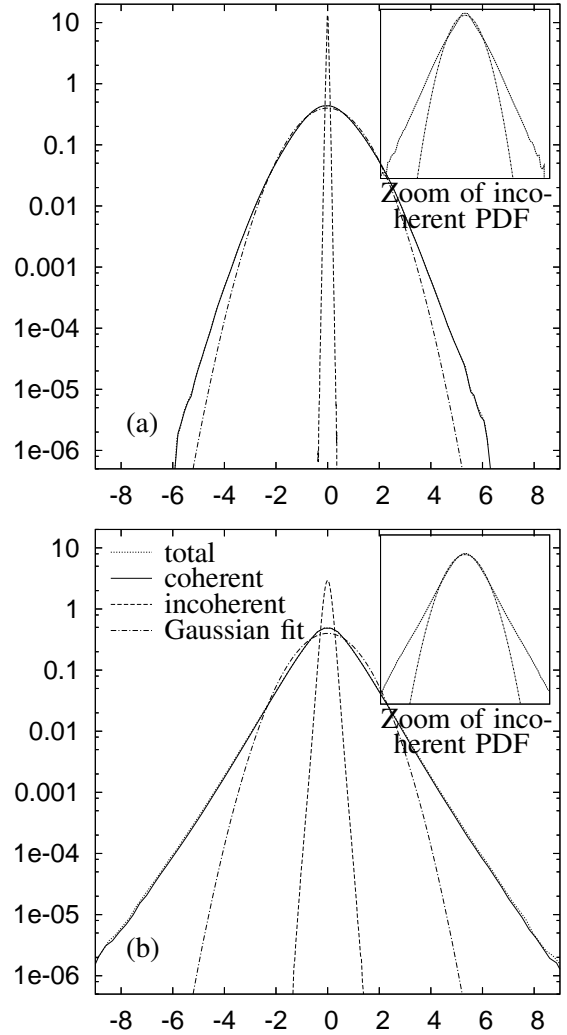


Figure 3. Normalised PDF of vorticity for the total, coherent and incoherent fields of (a) run A (anisotropic) and (b) run B (isotropic). Inset shows a zoom of the incoherent part with an appropriate Gaussian fit.

very similar to the ones of the total fields. The isotropic flow field shows an exponential distribution, in accordance with previous results obtained by CVE [5,6]. The vorticity PDFs of run A show a quasi-Gaussian distribution, possibly due to the action of the linear body forces on the flow. The vorticity PDFs of the incoherent parts (zoom shown in the inset of figure 3(a) and (b)) show a non-Gaussian distribution and have exponential tails, confirming significant differences to Gaussian noise both for runs A and B.

## CONCLUSIONS

We applied the CVE method to DNS data of rotating and stratified turbulence and to isotropic turbulence, both decaying, and compared the obtained results. In both cases the coherent part exhibits a multiscale behaviour with statistics close to the total flow. Compared to isotropic turbulence and despite higher Reynolds numbers, rotating and stratified turbulence shows a better compression rate and therefore a more coherent behaviour. This can partly be explained by the reduced cascade found in rotating and stratified turbulence, which is a consequence of linearising properties of rotation and stratification. Despite higher Reynolds numbers, the anisotropic field is therefore less turbulent in the conventional sense of disorder than isotropic turbulence with the similar turbulent energy density. The different ratios of energy to enstrophy due to different spectral energy distributions determine different Taylor micro scales for fluids of the same viscosity and with the same amount of energy. The incoherent part has a strongly reduced variance and is not Gaussian and does not show an equipartition in the spectral energy distribution. Future work will deal with quantifying a local, scale dependent anisotropy in wavelet space.

## ACKNOWLEDGMENTS

We thank IDRIS and CCRT for their continuous support in providing ample calculation time. L.L., M.F. and K.S. acknowledge financial support from the EU program IHP “Breaking complexity” (contract HPRN-CT 2002-00286).

## References

- [1] L. Liechtenstein, F.S. Godeferd, and C. Cambon. *Journal of Turbulence*, 6:1–18, 2005.
- [2] J. Pedlovsky *Geophysical Fluid Dynamics*, 1979.
- [3] L. Liechtenstein. PhD thesis, Ecole Centrale de Lyon, France, 2005.
- [4] C. Cambon. *Eur. J. Mech. B - Fluids*, 20:489–510, 2001.
- [5] M. Farge, G. Pellegrino, and K. Schneider. *Phys. Rev. Lett.*, 87(5):054501–1–054501–4, 2001.
- [6] O. Roussel, K. Schneider, and M. Farge. *Journal of Turbulence*, 6(11):1–15, 2005.
- [7] M. Farge. *Annu. Rev. of Fluid Mech.*, 24:395–457, 1992.